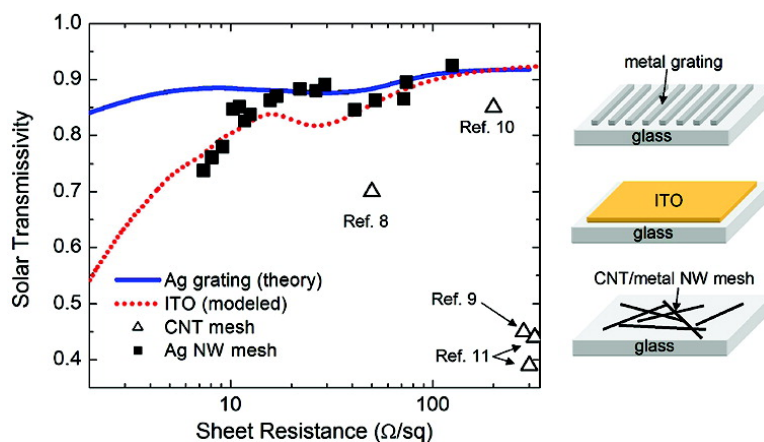


## Solution-Processed Metal Nanowire Mesh Transparent Electrodes

Jung-Yong Lee, Stephen T. Connor, Yi Cui, and Peter Peumans

*Nano Lett.*, **2008**, 8 (2), 689-692 • DOI: 10.1021/nl073296g

Downloaded from <http://pubs.acs.org> on January 13, 2009



### More About This Article

Additional resources and features associated with this article are available within the HTML version:

- Supporting Information
- Links to the 7 articles that cite this article, as of the time of this article download
- Access to high resolution figures
- Links to articles and content related to this article
- Copyright permission to reproduce figures and/or text from this article

[View the Full Text HTML](#)

# Solution-Processed Metal Nanowire Mesh Transparent Electrodes

Jung-Yong Lee,<sup>†</sup> Stephen T. Connor,<sup>‡</sup> Yi Cui,<sup>§</sup> and Peter Peumans<sup>\*,†</sup>

Department of Electrical Engineering, Stanford University, Stanford, California 94305,

Department of Chemistry, Stanford University, Stanford, California 94305, and

Department of Material Science and Engineering, Stanford University,

Stanford, California 94305

Received December 18, 2007

## ABSTRACT

Transparent conductive electrodes are important components of thin-film solar cells, light-emitting diodes, and many display technologies. Doped metal oxides are commonly used, but their optical transparency is limited for films with a low sheet resistance. Furthermore, they are prone to cracking when deposited on flexible substrates, are costly, and require a high-temperature step for the best performance. We demonstrate solution-processed transparent electrodes consisting of random meshes of metal nanowires that exhibit an optical transparency equivalent to or better than that of metal-oxide thin films for the same sheet resistance. Organic solar cells deposited on these electrodes show a performance equivalent to that of devices based on a conventional metal-oxide transparent electrode.

Thin-film optoelectronic devices make use of transparent, conductive thin-film electrodes to provide a low-resistance electrical contact to the active layers while not impeding coupling of light into and out of the devices. Transparent, conductive metal oxides such as indium tin oxide (ITO) and Al-doped zinc oxide are commonly used for this purpose, but they have a number of disadvantages. The cost of sputtered metal oxide thin films may be too high for applications in roll-to-roll processed solar cells and large-area organic light-emitting diodes (LEDs) for lighting applications.<sup>1</sup> When deposited on flexible substrates, the brittleness of metal oxides leads to film cracking when the substrate is bent, causing device failure.<sup>2</sup> In cases where a transparent electrode is required on top of organic active layers, the sputter deposition of ITO onto an organic material is known to cause damage to the underlying organic layers that leads to a decrease in device performance.<sup>3,4</sup> Finally, there is an inherent tradeoff between optical transparency and sheet resistance: thicker films (or higher doping concentrations) decrease not only the film sheet resistance but also the optical transparency, especially for sheet resistances  $R_{sh} < 15\Omega/\text{sq}$ , as shown in Figure 1 (red dotted line). For a sheet resistance of  $R_{sh} = 10\Omega/\text{sq}$ , a typical value for thin-film solar cells, the solar photon flux-weighted optical transparency of ITO on glass, is  $T_{\text{Solar}} = 80\%$ .

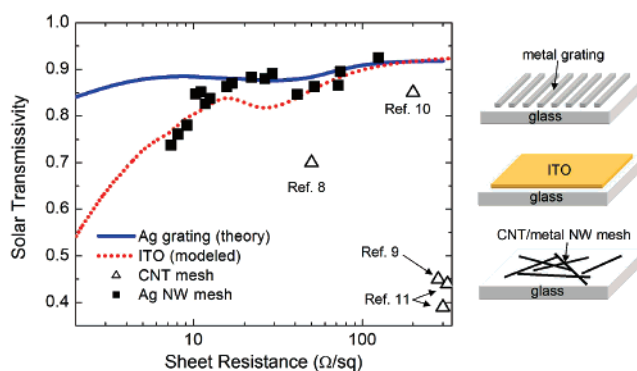


**Figure 1.** Solar photon flux-weighted transmissivity vs sheet resistance for Ag gratings (blue line), ITO (red dotted line), CNT meshes ( $\Delta$ ) and Ag nanowire meshes ( $\blacksquare$ ) deposited on a glass substrate. The data for the Ag gratings were obtained by finite-element modeling. The grating period is 400 nm, the Ag line width is 40 nm, and its thickness is varied. The data for ITO are computed based on optical constants for e-beam deposited ITO acquired using spectroscopic ellipsometry. The data for CNT meshes were obtained from the literature, and the Ag nanowire mesh data were obtained experimentally.  $T_{\text{Solar}}$  is calculated by integrating the product of the spectrally resolved transmittance with the spectrally resolved AM1.5 photon flux over the wavelength range  $\lambda = 400\text{--}800\text{ nm}$ .

Clearly, there is a need for an alternative approach to transparent conductive electrodes that has none of the disadvantages listed above. Random mesh networks of single wall carbon nanotubes (CNTs) deposited from solution were recently used as transparent electrodes for organic<sup>5,6</sup> and inorganic<sup>7</sup> photovoltaic cells. While this approach is potentially low-cost and the resulting electrodes are less prone to

\* To whom correspondence should be addressed. E-mail: ppeumans@stanford.edu.

<sup>†</sup> Department of Electrical Engineering.

<sup>‡</sup> Department of Chemistry.

<sup>§</sup> Department of Material Science and Engineering.

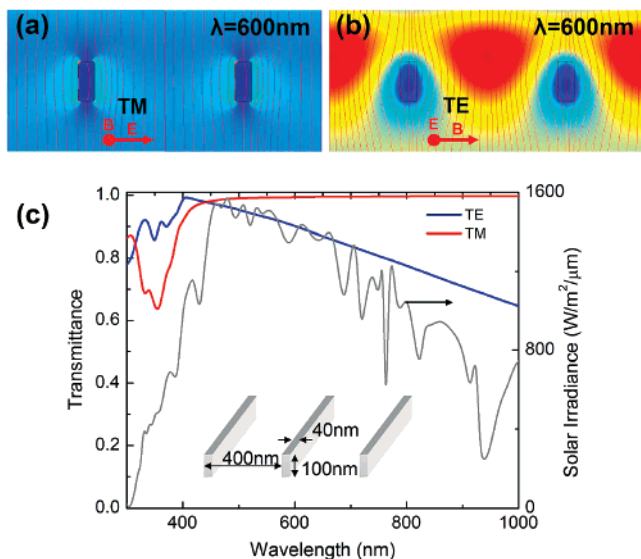


**Figure 2.** Absolute value of the modeled optical electric field (color) and power flow (red lines) for light with wavelength  $\lambda = 600$  nm incident on a freestanding 400-nm period, 40-nm line width, 100-nm high Ag grating for both the (a) TM and (b) TE polarization. Light is incident from the top. (c) Simulated transmittance vs wavelength for both the TE (blue line) and TM (red line) mode for the Ag grating shown in (a) and (b). The AM1.5 solar irradiance data are plotted for comparison (gray line).

failure when bending the substrate, the optical and electrical properties of CNT meshes<sup>8–12</sup> so far have been inferior to that of ITO, as shown in Figure 1 (open triangles). The relatively high sheet resistance of CNT meshes is attributed to a high tube–tube contact resistance between CNTs. Furthermore, CNT meshes contain a mixture of metallic and semiconducting CNTs, with the latter type contributing to optical absorption while not participating in lowering the sheet resistance.

Here, we investigate the use of nanostructured metal electrodes as transparent conducting electrodes. We first show that the optical transmission and sheet resistance of subwavelength periodic metal gratings are superior to those of ITO using electromagnetic modeling. We then show that random meshes of metal nanowires processed entirely from solution achieve a performance that approaches that of periodic metal gratings. A solar photon flux-weighted transmissivity of up to  $T_{\text{Solar}} = 85\%$  was achieved using such a solution-processed transparent thin-film electrode for a sheet resistance of  $R_{\text{sh}} = 10\Omega/\text{sq}$ . On flexible substrates, these electrodes can be bent to a radius of 4 mm without affecting the sheet resistance. Organic photovoltaic cells deposited onto a transparent metal nanowire mesh electrode exhibit improved photocurrents compared to identical cells fabricated on ITO-coated substrates.

Finite-element modeling<sup>13</sup> was used to calculate the optical transmittance of subwavelength metal gratings as a function of the geometric parameters of the gratings. In Figure 2a and b, the absolute value of the optical electric field (color) and optical power flow (red streamlines follow the Poynting vector) are shown for the TE and TM mode incident on a free-standing Ag grating in a vacuum with a period of 400 nm, a line width of 40 nm (geometric aperture of 90%), and

a height of 100 nm. The free space wavelength of the incident light is 600 nm. Assuming the conductivity of bulk Ag, the sheet resistance of this grating in the direction of the Ag lines is  $1.6\Omega/\text{sq}$ . The calculated optical transmittance is shown for the TE (blue solid line) and TM (red solid line) polarizations as a function of wavelength in Figure 2c. The solar spectrum is shown for reference (gray line). The transmittance of the TM mode exceeds the geometric aperture of 90% and is  $>99\%$  for  $\lambda > 500$  nm. The transmittance of the TE mode drops monotonously from 99% at  $\lambda = 400$  nm to 65% at  $\lambda = 1000$  nm, since the TE mode through the 90-nm-wide apertures becomes increasingly evanescent. The polarization-averaged solar photon flux-weighted transmissivity of these gratings of variable height on a glass substrate as a function of their sheet resistance is shown in Figure 1 (blue line). Our model calculations predict that metal gratings are substantially more transmissive than ITO for the same sheet resistance.

These models show that subwavelength metal gratings are good candidates for usage as transparent electrodes. This was recently demonstrated experimentally by Kang and Guo who used nanopatterned Ag gratings as a transparent electrode for organic LEDs with a performance comparable to that of ITO.<sup>14</sup> Despite the promise of nanopatterned metal gratings, their fabrication is likely to be too costly for applications in large-area, low-cost solar cells and LEDs. To address this issue, we have developed a low-cost method to fabricate transparent, nanostructured metal electrodes by casting suspensions of solution-synthesized metal nanowires.

Ag nanowires were synthesized by the reduction of Ag nitrate in the presence of poly(vinyl pyrrolidone) (PVP) in ethylene glycol.<sup>15</sup> The resulting Ag nanowires are  $8.7 \pm 3.7$   $\mu\text{m}$  long and have a diameter of  $103 \pm 17$  nm. To fabricate transparent electrodes using nanowire suspensions, a volume of the nanowire suspension is dropped on a glass substrate with 100-nm-thick prepatterned Ag contact pads and is allowed to dry in air for 10 min while agitated on a shaker. The resulting films are random meshes of Ag nanowires without significant bundling of wires that are uniform over the area of the substrate, as shown in the scanning electron microscope (SEM) images in Figure 3a. The initial sheet resistance of the nanowire mesh electrodes is  $>1$   $\text{k}\Omega/\text{sq}$  due to the presence of the 1-nm- to 3-nm-thick PVP surfactant layer. As shown in Figure 3b, annealing of the meshes at a temperature of 200 °C results in a steep drop of the sheet resistance (measured at the annealing temperature) by more than an order of magnitude from  $R_{\text{sh}} > 1$   $\text{k}\Omega/\text{sq}$  to  $R_{\text{sh}} \approx 100\Omega/\text{sq}$  after 20 min. The reduction in  $R_{\text{sh}}$  is attributed to the flowing and partial decomposition of the PVP which allows the Ag nanowires to make contact and fuse together. Continued annealing at 200 °C for more than 40 min leads to a gradual increase in  $R_{\text{sh}}$  as the Ag nanowires coalesce into disconnected droplets. The lowest temperature at which a low  $R_{\text{sh}}$  is achieved is 180 °C.

The  $R_{\text{sh}}$  of a metal nanowire mesh depends on the wire length,  $L$ , wire resistance,  $R_{\text{w}}$ , the wire–wire contact resistance,  $R_{\text{c}}$ , and wire aerial density,  $D$ . To understand the factors that limit  $R_{\text{sh}}$ , we evaluated its dependence on the

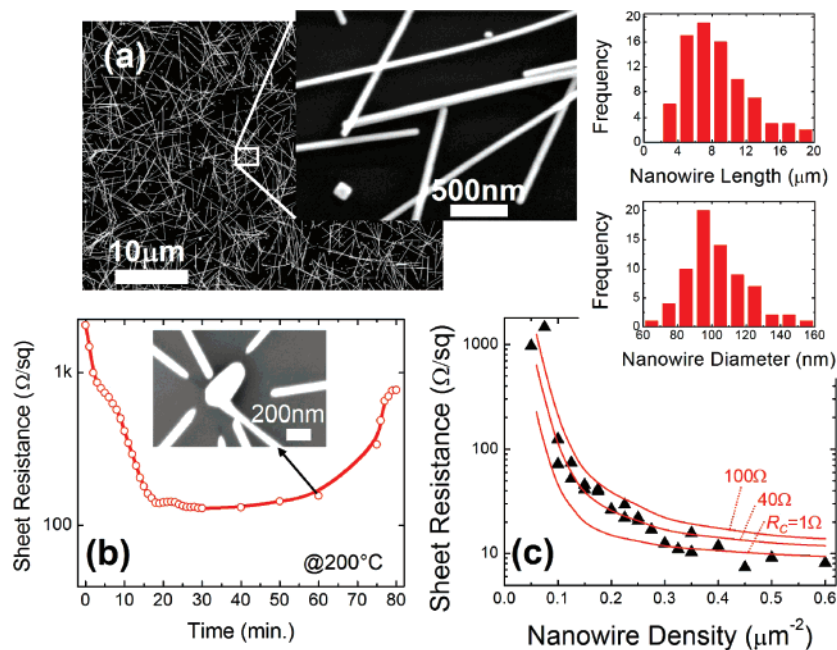


**Figure 3.** (a) SEM images of an Ag nanowire mesh on a silicon substrates. The Ag nanowire length and diameter histogram is also shown. (b) Sheet resistance vs annealing time for an Ag nanowire mesh annealed at 200 °C. After ~40 min of annealing, the Ag nanowires start to coalesce, breaking the electrical connections, as shown in the SEM image in the inset. The line is a guide to the eye. (c) Experimentally determined sheet resistance vs Ag nanowire aerial density (triangles) and theoretical results for a nanowire length of 8.7  $\mu\text{m}$  and diameter of 103 nm ( $R_W = 18 \Omega$ ) and for different values of contact resistances  $R_C = 1, 40,$  and  $100 \Omega$ .

above parameters using computer generated random meshes since no analytical models are known.<sup>16</sup> The distribution of Ag nanowire lengths and diameters determined from SEM images is shown in Figure 3a. The average length is  $L_{\text{avg}} = 8.7 \mu\text{m}$ , and the average diameter is  $d_{\text{avg}} = 103 \text{ nm}$ . Assuming the bulk resistivity of Ag is  $\rho = 1.6 \mu\Omega\cdot\text{cm}$ , the average wire has a resistance of  $R_{W,\text{avg}} = 18 \Omega$ . In the simulated nanowire meshes, all wires were assumed to be of length  $L = L_{\text{avg}}$  with a wire resistance of  $R_W = R_{W,\text{avg}}$ . In Figure 3c, the experimentally obtained  $R_{\text{sh}}$  for Ag nanowire meshes with varying wire density,  $D$ , determined from SEM images, is compared with model calculations assuming  $R_C = 1, 40,$  and  $100 \Omega$ . The data agree well with the model calculations for  $R_C = 40 \Omega$  for  $D < 0.3 \mu\text{m}^{-2}$ . For  $D > 0.3 \mu\text{m}^{-2}$ , the data are better described by model calculations for  $R_C = 1 \Omega$ . This is attributed to the formation of many parallel connections with the lowest resistance connections dominating the overall resistance.

A Ag nanowire mesh with  $R_{\text{sh}} = 11.8 \Omega/\text{sq}$  was deposited on 63.5- $\mu\text{m}$ -thick Kapton tape to evaluate changes in  $R_{\text{sh}}$  when the substrate is bent. No changes in  $R_{\text{sh}}$  larger than 1% were measured for bending radii down to 4 mm, and no changes were observed when the substrate relaxed back to the planar shape.

The random nature of the Ag nanowire meshes leads to substantial scattering of incident light. Approximately 20% of the transmitted light is scattered over angles  $> 10^\circ$ . Since the scattered light contributes to photocurrent generation in solar cells, the optical transmittance of the Ag nanowire meshes was measured using an integrating sphere. The spectrally resolved diffuse transmittance for two Ag nanowire meshes is shown in Figure 4a. The solar photon flux-

weighted transmissivity,  $T_{\text{Solar}}$ , is plotted as a function of the nanowire mesh aerial density in the inset of Figure 4a (triangles) and as a function of its  $R_{\text{sh}}$  in Figure 1 (squares). For a given  $R_{\text{sh}}$ , the Ag nanowire meshes on glass exhibit a  $T_{\text{Solar}}$  that is comparable to or higher than that of ITO on glass. Given that the Ag nanowire meshes can potentially be deposited at much lower cost because they are processed from solution, require only a moderate temperature step of 180–200 °C, and do not fail upon bending of the substrate, we conclude that they are an attractive replacement for metal-oxide transparent electrodes in many applications.

To evaluate the potential of metal nanowire mesh transparent electrodes for use in devices, small molecular weight organic photovoltaic cells were deposited onto Ag nanowire mesh electrodes with  $T_{\text{Solar}} = 86\%$  and  $R_{\text{sh}} = 16 \Omega/\text{sq}$ . The Ag nanowire mesh was coated with a layer of poly(3,4-ethylenedioxythiophene) poly(styrenesulfonate) (PEDOT:PSS) by spin-coating after annealing to adjust the work-function. The presence of the transparent, conductive PEDOT:PSS layer ensures that holes generated in the organic solar cell are collected efficiently despite the relatively large distance between the Ag nanowires compared to the thickness of the organic layers. On top of the Ag nanowire–PEDOT:PSS composite transparent electrode, a bilayer solar cell<sup>17</sup> with the following layer structure was deposited by vacuum sublimation: 45 nm of copper phthalocyanine (CuPc)/45 nm of 3,4,9,10-perylenetetracarboxylic bisbenzimidazole (PTCBI)/10 nm of bathocuproine (BCP)/100 nm of Ag. The same device structure was simultaneously deposited on a conventional ITO transparent electrode on glass for comparison. The thickness of these devices is larger than the optimal

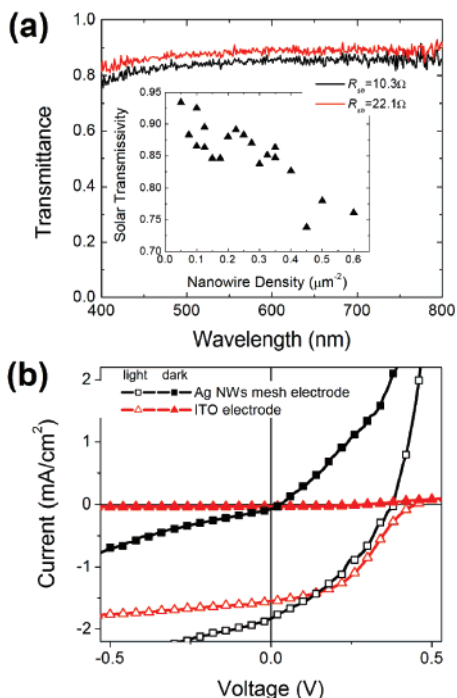


**Figure 4.** (a) Diffuse optical transmittance for two Ag nanowire meshes with  $R_{sh} = 10.3 \Omega/\text{sq}$  (black line) and  $R_{sh} = 22.1 \Omega/\text{sq}$  (red line). The solar photon flux-weighted transmissivity of these two films is  $T_{\text{Solar}} = 84.7\%$  and  $T_{\text{Solar}} = 88.3\%$ , respectively. Inset: Solar photon flux-weighted transmissivity as a function of Ag nanowire mesh aerial density (triangles). (b) Current density vs voltage for organic photovoltaic cells with device structure 45 nm CuPc/45 nm PTCBI/10 nm BCP/100 nm Ag on an Ag nanowire mesh (squares) and ITO (triangles) in the dark (filled symbols) and under  $65 \text{ mW}/\text{cm}^2$  AM1.5 illumination (open symbols).

thickness in order to prevent shorts due to the topography of the 100-nm-diameter Ag nanowire meshes.

In Figure 4b, the current–voltage characteristics of the bilayer photovoltaic devices in the dark and under  $65 \text{ mW}/\text{cm}^2$  AM1.5 illumination are shown. The short circuit current density,  $J_{\text{SC}}$ , is  $1.83 \text{ mA}/\text{cm}^2$  for the devices deposited on the Ag nanowire mesh electrode and  $1.54 \text{ mA}/\text{cm}^2$  for devices on ITO. The 19% increase in short circuit current for the devices on the Ag nanowire mesh is attributed to the higher optical transmissivity, improved optical path length due to scattering of incident light, increased roughness of the donor–acceptor interface, and possibly a local enhancement of the optical intensity near the metal nanowires. The power conversion efficiencies of the devices on the random Ag nanowire mesh and ITO electrode are 0.38% and 0.42%, respectively. The lower efficiency of the device on the Ag nanowire mesh is chiefly due to a higher dark current that is likely the result of current shunt paths due to the roughness of the Ag nanowire electrode. The efficiency of these devices is well below the state of the art for this material system,<sup>18</sup> since thick, nonoptimized devices were used. We anticipate that application of solution-processed Ag nanowire mesh electrodes to today’s best organic solar cells will lead to improved efficiencies.

In conclusion, we demonstrated that Ag nanowire mesh electrodes can be used as transparent electrodes with a

performance that exceeds that of commonly used metal oxides. Moreover, these electrodes are fabricated entirely from solution and require only a low temperature annealing step that is compatible with most plastics. The nanowire meshes are compatible with flexible substrates, and organic solar cells based on such nanowire meshes were shown to exhibit a 19% higher photocurrent. We anticipate that the application of metal nanowire mesh transparent electrodes to a wide variety of devices, including organic solar cells, will lead to lower cost fabrication and improved performance.

**Acknowledgment.** This work was supported by the National Science Foundation, the Stanford Global Climate and Energy Project, the Center for Integrated Systems at Stanford, and the Center for Probing the Nanoscale at Stanford. J.-Y.L. would like to thank The Korea Foundation for Advanced Studies for its support. S.T.C. acknowledges the support from an NSF Graduate Fellowship. Author Contributions: J.-Y.L. fabricated all samples and devices. S.T.C. synthesized all the nanowire suspensions. All authors contributed to the manuscript.

## References

- (1) Forrest, S. R. The path to ubiquitous and low-cost organic electronic appliances on plastic. *Nature* **2004**, *428*, 911–918.
- (2) Chen, Z.; Cotterell, B.; Wang, W.; Guenther, E.; Chua, S.-J. A mechanical assessment of flexible optoelectronic devices. *Thin Solid Films* **2001**, *394*, 201–205.
- (3) Gu, G.; Bulovic, V.; Burrows, P. E.; Forrest, S. R.; Thompson, M. E. Transparent organic light emitting devices. *Appl. Phys. Lett.* **1996**, *68*, 2606–2608.
- (4) Kim, H.-K. *et al.* Plasma damage-free sputtering of indium tin oxide cathode layers for top-emitting organic light-emitting diodes. *Appl. Phys. Lett.* **2005**, *86*, 183503–183505.
- (5) Wu, Z. *et al.* Transparent, Conductive Carbon Nanotube Films. *Science* **2004**, *305*, 1273–1276.
- (6) Zhang, M. *et al.* Strong, transparent, multifunctional, carbon nanotube sheets. *Science* **2005**, *309*, 1215–1219.
- (7) Barnes, T. M. *et al.* Single-wall carbon nanotube networks as a transparent back contact in CdTe solar cells. *Appl. Phys. Lett.* **2007**, *90*, 243503–243505.
- (8) Lagemaat, J. *et al.* Organic solar cells with carbon nanotubes replacing  $\text{In}_2\text{O}_3:\text{Sn}$  as the transparent electrode. *Appl. Phys. Lett.* **2006**, *88*, 233503.
- (9) Pasquier, A. D. *et al.* Conducting and transparent single-wall carbon nanotube electrodes for polymer-fullerene solar cells. *Appl. Phys. Lett.* **2005**, *87*, 203511.
- (10) Rowell, M. W. *et al.* Organic solar cells with carbon nanotube network electrodes. *Appl. Phys. Lett.* **2006**, *88*, 233506.
- (11) Kaempgen, M.; Duesberg, G. S.; Roth, S. Transparent carbon nanotube coatings. *Appl. Surf. Sci.* **2005**, *252*, 425–429.
- (12) Gruner, G. Carbon nanotube films for transparent and plastic electronics. *J. Mater. Chem.* **2006**, *16*, 3533–3539.
- (13) COMSOLAB, Comsol multiphysics, 1 New England Executive Park Suite 350, Burlington, MA 01803 2007.
- (14) Kang, M.-G.; Guo, L. J. Nanoimprinted Semitransparent Metal Electrodes and Their Application in Organic Light-Emitting Diodes. *Adv. Mater.* **2007**, *19*, 1391–1396.
- (15) Tao, A. *et al.* Langmuir–Blodgett silver nanowire monolayers for molecular sensing using surface-enhanced Raman spectroscopy. *Nano Lett.* **2003**, *3*, 1229–1233.
- (16) Kumar, S.; Murthy, J. Y.; Alam, M. A. Percolating conduction in finite nanotube networks. *Phys. Rev. Lett.* **2005**, *95*, 066802.
- (17) Tang, C. W. Two-layer organic photovoltaic cell. *Appl. Phys. Lett.* **1986**, *48*, 183–185.
- (18) Peumans, P.; Uchida, S.; Forrest, S. R. Efficient bulk heterojunction photovoltaic cells using small-molecular-weight organic thin films. *Nature* **2003**, *425*, 158–162.

NL073296G